

Caloric effects around phase transitions in magnetic materials described by *ab initio* theory: The electronic glue and fluctuating local moments

Eduardo Mendive-Tapia^{1,2} and Julie B. Staunton^{*2}

¹*Department of Computational Materials Design, Max-Planck-Institut für Eisenforschung GmbH, 40237 Düsseldorf, Germany*

²*Department of Physics, University of Warwick, Coventry CV4 7AL, U.K.*

(Dated: 27 May 2020)

We describe magneto-, baro- and elastocaloric effects (MCEs, BCEs and eCEs) in materials which possess both discontinuous (first-order) and continuous (second-order) magnetic phase transitions. Our *ab initio* theory of the interacting electrons of materials in terms of disordered local moments (DLMs) has produced explicit mechanisms for the drivers of these transitions and here we study associated caloric effects in three case studies where both types of transition are evident. Our earlier work had described FeRh's magnetic phase diagram and large MCE. Here we present calculations of its substantial BCE and eCE. We describe the MCE of dysprosium and find very good agreement with experimental values for isothermal entropy (ΔS_{iso}) and adiabatic temperature (ΔT_{ad}) changes over a large temperature span and different applied magnetic field values. We examine the conditions for optimal values of both ΔS_{iso} and ΔT_{ad} that comply with a Clausius-Clapeyron analysis, which we use to propose a promising elastocaloric cooling cycle arising from the unusual dependence of the entropy on temperature and biaxial strain found in our third case study - the Mn₃GaN antiperovskite. We explain how both ΔS_{iso} and ΔT_{ad} can be kept large by exploiting the complex tensile strain-temperature magnetic phase diagram which we had earlier predicted for this material and also propose that hysteresis effects will be absent from half the caloric cycle. This rich and complex behavior stems from the frustrated nature of the interactions among the Mn local moments.

I. INTRODUCTION

The extent and state of magnetic order can change dramatically when a material is subjected to an external stimulus such as a magnetic field, applied pressure or strain. Magneto- and mechano-(baro- and elasto-)caloric effects that accompany these changes underpin the design of cooling cycles and attractive forms of solid state cooling¹⁻³. At a fundamental level the versatility of magnetic materials for such applications comes from the complex glue of electrons which both binds the nuclei of a material together and generates the magnetism. The spins of the septillions of interacting electrons cause atomic-scale, relatively long-lived magnetic moments to emerge from the electronic fluid and the moments' behavior fixes properties such as the overall magnetization along with its resilience and response to magnetic fields. At high temperatures the moments disorder so that they average out to produce a low or zero magnetisation. At lower temperatures ordered patterns of the moments form changing the material's properties.

Over the last few years we have developed *ab initio* computational modelling which accurately accounts for this physics^{4,5}. It describes how intrinsic magnetic properties change as the temperature is varied, a magnetic field applied, the material is compressed or strained etc. We can model both smooth (second-order) and sharp (first-order) transitions between different magnetic moment ordered patterns in multicomponent materials and calculate quantities to gauge usefulness for multicalorics and energy-efficient cooling applications. Our theory models the material at the sub-nanoscale, where the behavior of the many interacting electrons is carefully ac-

counted for, to produce interactions among the magnetic moments. A statistical mechanical treatment describes quantitatively and directly the caloric properties such as the changes in entropy and temperature that happen when a magnetic field and/or mechanical stress is applied.

Our recent applications of the theory include the first-order ferromagnetic (FM) to antiferromagnetic (AFM) transition around room temperature and large magnetocaloric effect in the much studied FeRh ordered alloy⁶, metamagnetic critical fields in CoMnSi-based alloys⁷, FM, AFM and canted magnetic phases in lanthanide intermetallics⁸, the magnetic field and temperature induced transitions between long period helical AFM, fan and FM phases in the heavy lanthanide elements⁹, the frustrated magnetism and mechanocaloric effects in the Mn-based antiperovskite nitrides¹⁰, temperature dependent permanent magnetic properties⁵, and transitions between paramagnetic, ferrimagnetic, collinear AFM and non-collinear triangular AFM phases in the Mn₃A class of materials together with the influence of strain and volume change⁴.

In this paper we outline the underlying theory and computational approach (Sect. II). We illustrate the theory with a description of mechanocaloric effects in FeRh in the vicinity of its FM-to-AFM first order phase transition when subjected to pressure and/or strain (Sect. III). We then present results which show both the complexity and potential for exploitation for solid state cooling of the caloric effects that can occur in a material with a magnetic phase diagram containing both first- and second-order phase transitions. We discuss the implications on these aspects within the context of our modelling of the

magnetocaloric effect in the heavy rare earth elements (Sect. IV). These examples serve as an introduction to our proposals for new cooling cycles which we illustrate by a further case study based on the elastocaloric effects of the antiperovskite nitride Mn_3GaN (Sect. V). We conclude with an outlook for the role of *ab initio* predictive modelling in the multicalorics field.

II. TEMPERATURE-DEPENDENT MAGNETIC PROPERTIES FROM FIRST PRINCIPLES THEORY.

The *ab initio* modelling is based on the premise that important magnetic fluctuations in a material can be modelled as ‘local moments’, a picture captured by a generalization of Density Functional Theory (DFT) for non-collinear spin polarization. For itinerant electrons a separation of time scales between fast and slow electronic degrees of freedom causes local moments with slowly varying orientations, $\{\hat{\mathbf{e}}_n\}$, to emerge from the interacting electrons of a material with N atomic sites at positions $\{\mathbf{R}_n\}$ ^{4-6,11,12}. This means that ‘disordered local moments’ (DLMs) are sustained by and influence the faster electronic motions. Their interactions with each other depend on the type and extent of the long-range magnetic order through the associated spin-polarized electronic structure⁶ which itself adapts to the extent of magnetic order. For materials with rare earth lanthanide (RE) components the strongly correlated 4f electrons are treated with our self interaction correction (SIC) approach which is parameter free and incorporates Hund’s rules naturally¹³. The crucial RE contribution to the

magnetic anisotropy is accounted for using crystal field theory, calculating the crystal field coefficients within DFT using a robust numerical method¹⁴.

Ensemble averages over all the appropriately weighted noncollinear local moment orientational configurations are required for a realistic evaluation of the system’s magnetic properties. A set of magnetic order parameters, $\{\mathbf{m}_n = \langle \hat{\mathbf{e}}_n \rangle\}$, specify the type and extent of magnetic order. An *ab initio* Gibbs free energy is given by the following expression:

$$\mathcal{G}_1 = -TS + \Omega(\{\mathbf{m}_n\}, \mathbf{H}, P, \sigma_{\alpha\beta}, T) + \mathcal{G}_{RE}(\mathbf{B}_{eff}(\{\mathbf{m}_n\}), \mathbf{H}, P, \sigma_{\alpha\beta}, T) \quad (1)$$

where $\Omega(\{\mathbf{m}_n\}, \mathbf{H}, P, \sigma_{\alpha\beta}, T)$ is a magnetic energy of the material, which can include the effect of an external magnetic field \mathbf{H} , applied pressure P and mechanical stress $\sigma_{\alpha\beta}$. $\Omega(\{\mathbf{m}_n\}, \mathbf{H}, P, \sigma_{\alpha\beta}, T)$ is obtained as an average over local moment configurations of the grand potential of the itinerant, interacting electrons of a material with spin polarization constrained to $\{\hat{\mathbf{e}}_n\}$ ^{4-6,11,12}. $S = \sum_n S_n$ is the total entropy of the local moments and $\mathcal{G}_{RE}(\mathbf{B}_{ex}(\{\mathbf{m}_n\}), \mathbf{H}, P, \sigma_{\alpha\beta}, T)$ describes the free energy of localized RE-4f electrons determined by an atomic-like Hamiltonian which includes the effective magnetic field $\mathbf{B}_{ex}(\{\mathbf{m}_n\})$ from the other electrons in the system and the crystal field^{5,14}. The equilibrium state of the system for specific values of the temperature, T , and applied field \mathbf{H} and/or P and $\sigma_{\alpha\beta}$, is given by the set of order parameters $\{\mathbf{m}_n\}$ which minimizes the Gibbs free energy function \mathcal{G}_1 ^{4,6}.

The magnetic energy can be expressed in the form

$$\Omega(\{\mathbf{m}_n\}, \mathbf{H}, P, \sigma_{\alpha\beta}, T) = \Omega_0 + f^{(2)}(\{\mathbf{m}_n\}) + \sum_{a>2} f^{(a)}(\{\mathbf{m}_n\}) - \mathbf{H} \cdot \sum_n \mu_n \mathbf{m}_n + \frac{1}{2} C_{\alpha\beta\gamma\kappa} \epsilon_{\alpha\beta} \epsilon_{\gamma\kappa} + \sigma_{\alpha\beta} \epsilon_{\alpha\beta}, \quad (2)$$

where Ω_0 is a constant, μ_n is the size of a local moment on a site n and $\{f^{(a)}\}$ are order a functions of $\{\mathbf{m}_n\}$ which can depend on the lattice deformation, described by the strain tensor $\epsilon_{\alpha\beta}$ and the energy cost of mechanical stress given by the elastic moduli $C_{\alpha\beta\gamma\kappa}$ term. The $f^{(2)}$ describe pairwise correlations between local moments and are obtained rigorously from an analysis of the linear response of the paramagnetic state to small applied fields⁴. They identify the dominant pair interactions between moments and the potentially most stable magnetic phases in a material, which can include non-collinear and long-period states in complex multi-atom unit cells. The $f^{(a>2)}$ describe higher order effects and produce a picture of effective ‘multi-site’ magnetic interactions depending on how the electronic structure evolves with the state and extent of magnetic order. They are extracted from a linear regression fitting procedure to data produced by a large number of calculations for prescribed magnetic

orders $\{\mathbf{m}_n\}$ ^{4-6,9,10,13} and which exploits the symmetries of the feasible magnetic states.

In general, a caloric effect is quantified by the isothermal entropy change, ΔS_{iso} , and the adiabatic temperature change, ΔT_{ad} , induced in the thermodynamic conjugate of the external field applied and/or removed. Our DFT-DLM theory can directly provide the total entropy as a function of the state of magnetic order, as well as the dependence on temperature, applied stimuli and crystal structure. It predicts the entropy changes formulated as a sum of three components. The first two are natural outputs from the DLM picture and are calculated directly. There is the contribution from the orientational disorder of the local moments, $\Delta S_{mag} = \Delta(\sum_n S_n)$,^{4,15} and then an electronic piece estimated from the entropy change from alterations in the vicinity of the Fermi energy E_F of the electronic density of states (DOS), i.e. $\frac{\pi^2}{3} k_B^2 T n(\{\mathbf{m}_n\}, E_F)$ where $n(\{\mathbf{m}_n\}, E_F)$ is the DOS at

the Fermi energy in a magnetic state specified by order parameters $\{\mathbf{m}_n\}$. The third component contains the lattice vibrational entropy and is currently estimated from a simple Debye model relying on θ_D the Debye temperature, which can be obtained from experiment or other first principles sources¹⁶.

III. BARO- AND ELASTOCALORIC EFFECTS IN IRON-RHODIUM.

For roughly stoichiometric compositions $\text{Fe}_{50}\text{Rh}_{50}$ orders into a paramagnetic (PM) B2 (CsCl) alloy phase. On cooling the alloy undergoes a second-order transition into a ferromagnetically ordered phase at a T_c around 700K followed by its famous first-order ferromagnetic-to-antiferromagnetic (FM-AFM) transition at T_t . This FM-AFM magnetic transformation occurs near room temperature and shows one of the largest recorded magnetocaloric effects (MCEs) around T_t ^{17,18} which deteriorates on subsequent magnetic and thermal cycling. The FM-AFM transition has been extensively studied, e.g.^{18–25} and has been shown to be profoundly composition dependent. It vanishes in alloys with as little as a 2% iron excess or deficiency and T_t varies strongly with sample preparation, i.e. the extent of the long range B2 order. Building on several DFT studies^{26–30} we applied the theory described above and were able to model the salient features of the alloy's behavior and obtain good agreement with experiment. We described *ab initio* the magnetic phase diagram of FeRh, its MCE and the hypersensitivity of the FM-AFM transition to compositional variation⁶.

The theory modelling produces a picture of local moments forming on the cubic sublattice occupied by Fe atoms which interact antiferromagnetically with each other. There is a competing energy benefit however if they align ferromagnetically so that the electronic density around the Rh sites on the other interpenetrating cubic sub-lattice becomes spin-polarized. A small number of Fe atoms replacing Rh ones greatly strengthen this ferromagnetic effect. It is this exquisite balance between AFM and FM mechanisms and their robust electronic origins which are at the centre of the compositional hypersensitivity and large negative MCE at the AFM-FM discontinuous transition⁶. Here we report that the competition between the FM and AFM interactions are also affected by the separations between Fe nearest neighbors and lead to pronounced barocaloric and elastocaloric effects around the FM-AFM discontinuous transition. We point out however that the modelling shows that magnetostructural effects are not the principal drivers of the transition but instead are consequences of it.

The antiferromagnetic interactions between neighboring Fe atoms strengthen when their separations decrease as found by other authors²⁶. We model the effect of pressure and compressive biaxial strain on the transition by assuming a Poisson ratio of $\frac{1}{3}$ and bulk and Young mod-

uli both equal to 1800kbar as reasonable empirical values. The description of lattice fluctuations uses a Debye temperature of 400K. We estimate a spontaneous volume reduction of 0.7% at the FM-AFM transition and calculate the variation of T_t with pressure to be 3K/kbar. Table I summarises our results for the magnetocaloric, barocaloric (BCE) and elastocaloric (eCE) effects in iron rhodium together with a comparison with experimental data^{2,17,18,31–33}. The MCE is calculated for an application of a 2 tesla magnetic field, the BCE for application of 1 kbar of pressure and the eCE for the application of a compressive biaxial strain of 0.05%. There is fair agreement in both the magnitudes and the signs of these values between theory and experiment, e.g. we find that the MCE is inverse and the mechanocaloric (compressive) effects are conventional.

IV. THE MAGNETOCALORIC EFFECT IN THE HEAVY RARE EARTH ELEMENTS

The magnetism of the heavy rare earth (HRE) elements, from gadolinium to lutetium, is composed of a varied range of magnetic phase transitions between complicated, incommensurate AFM and FM states, triggered by both temperature changes and the application of a magnetic field³⁴. Although the HREs share a common valence electronic structure their magnetic phases can be very different. In Ref.⁹ we demonstrated that a major part of this complex magnetic phase landscape arises from the response of the valence electrons, via a Fermi surface topological change, to temperature-dependent f-electron magnetic moment order and its link to quartic order magnetic correlations, $f^{(4)}$ (see Eq. 2). A generic temperature-magnetic field phase diagram of a heavy lanthanide was obtained by minimizing the Gibbs free energy in Eq. (1), as shown in Fig. 1(d) for Dy and experimentally observed for Tb^{35–38}, Dy^{39–41}, and Ho^{42,43}. In the absence of a magnetic field the PM state of these lanthanide metals becomes unstable to the formation of a helical antiferromagnetic (HAFM) ordering through a second-order transition at T_N . Lowering the temperature sufficiently triggers a first-order transition to a FM phase at T_t which is stable down to $T = 0\text{K}$. Whilst the application of a magnetic field \mathbf{H} only spin-polarizes further the FM state below T_t , it triggers complex magnetic stabilities when applied between T_t and T_N where the helical structure is stable. For increasing values of \mathbf{H} the HAFM phase firstly distorts and then discontinuously transforms to a fan magnetic phase³⁴. Further increase of the applied magnetic field continuously stabilizes a FM state.

Such a complex magnetic phase diagram contains both second- and first-order magnetic phase transitions which vary differently as a magnetic field is applied. Here we focus on the associated magnetocaloric effect (MCE) which shows a complicated dependence on temperature spanning the large interval between T_N and T_t . In panels

	ΔS_{iso}^{exp} (Jkg ⁻¹ K ⁻¹)	ΔS_{iso}^{theo} (Jkg ⁻¹ K ⁻¹)	ΔT_{ad}^{exp} (K)	ΔT_{ad}^{theo} (K)
MCE ($H = 0 \rightarrow 2T$)	between 12 and 20	+22	-7	-7
BCE ($P = 0 \rightarrow 1\text{kbar}$)	-12	-23	between 0 and +10	+3
eCE (strain= 0 \rightarrow 0.05%)	-8	-23	+3	+5

TABLE I. The MCE, BCE and eCE (compressive) of FeRh from the theory and comparison with experimental values (MCE^{2,17,18,31,32}, BCE³² and eCE³³).

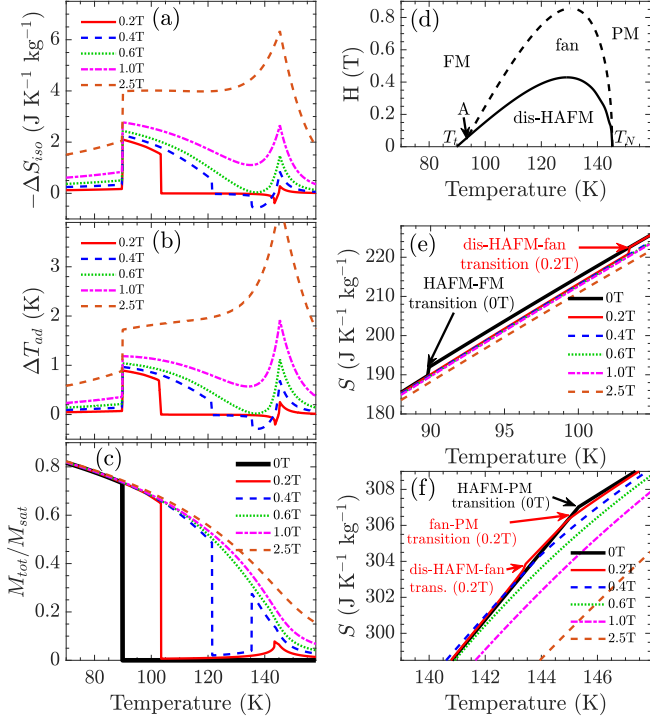


FIG. 1. (a) Isothermal entropy change and (b) adiabatic temperature change obtained for Dy as functions of temperature produced by the application of a magnetic field from $\mathbf{H} = \mathbf{0}$ to increasing values up to 2.5 Tesla. (c) The total magnetization along the ferromagnetic component, which is also the direction of the magnetic field, normalized to the saturation value at zero temperature M_{sat} . (d) The *ab-initio* temperature-magnetic field phase diagram of Dy as obtained in Ref.⁹. Discontinuous (continuous) black lines indicate first-(second)-order magnetic phase transitions. Panels (e) and (f) show the entropy against temperature around T_t and T_N , respectively, for the same increasing values of the applied field.

(a) and (b) of Fig. 1 we show the isothermal entropy change, ΔS_{iso} , and adiabatic temperature change, ΔT_{ad} , obtained for Dy, which are in very good qualitative and quantitative agreement with experiment⁴⁰. To describe the lattice vibrations we used a Debye temperature of $\theta_D = 180\text{K}$ ⁴⁴⁻⁴⁶. Values of ΔS_{iso} and ΔT_{ad} obtained for Gd, which only shows a single PM-FM second-order transition, also match experiment very well¹⁵. In the case of Dy we observe that for smaller values of the mag-

netic field (below 0.2T) the magnetocaloric response is much larger around T_t compared to T_N , as these are first- and second-order transitions respectively. Interestingly, the MCE is conventional at T_t and above T_N , but inverse below T_N (see Fig. 1(a,b)). Such a behavior can be traced back to the temperature dependence of the total magnetization, shown in Fig. 1(c). For negative or positive values of $\frac{\partial M_{tot}}{\partial T}$ at small applied fields the MCE is conventional ($\Delta S_{iso} < 0$) or inverse ($\Delta S_{iso} > 0$), respectively. This directly follows from the fundamental relation $\Delta S_{iso} = \int_0^{\mathbf{H}} \frac{T}{C} \frac{\partial M_{tot}}{\partial T} d\mathbf{H}$ ⁴⁷, where C is the heat capacity at constant applied field. The only qualitatively behavior not captured by our theory in comparison with experiment is observed immediately above T_t , for which the gradient of the MCE with temperature is negative, i.e. $-\frac{\partial \Delta S_{iso}}{\partial T} < 0$ and $\frac{\partial \Delta T_{ad}}{\partial T} < 0$, instead of positive (see Fig. 22 of Ref.⁴⁰). This discrepancy is caused by a consistently incorrect sign of $\frac{\partial M_{tot}}{\partial T}$ in the vicinity above T_t for low values of \mathbf{H} , which is positive in our calculations and negative in experiment. After closely comparing the experimental and theoretical magnetic phase diagrams of Dy⁴⁰, we consider that such a minor detail could be related to possible spin-flops or similar magnetic transitions not captured by our theory and linked to subtle magnetization changes.

Inspecting Fig. 1(b) reveals that for large magnetic fields above 0.6T the adiabatic temperature change around the second-order transition T_N becomes bigger than the one observed around the first-order T_t , as found in experiment (see Figs. 23 and 26 of Ref.⁴⁰). This observation can be understood by considering the Clausius-Clapeyron equation^{2,47,48}

$$\Delta S_{iso} \propto \left[\frac{dT_{FOT}}{dx} \right]^{-1}, \quad (3)$$

where T_{FOT} is the temperature at which the first-order transition occurs and \mathbf{x} is the applied field for the conjugate displacement, i.e. a magnetic field \mathbf{H} or a mechanical stress $\sigma_{\alpha\beta}$ for magnetization and strain variations, respectively. Typically, the temperature-dependent entropy behavior observed around first-order magnetic phase transitions is as shown in Fig. 2². Panels (a) and (b) show the limits in which $\frac{dT_{FOT}}{dx}$ is very small and very large, respectively. Case (a) allows for wide values of ΔS_{iso} in exchange of small adiabatic temperature changes ΔT_{ad} . Increasing $\frac{dT_{FOT}}{dx}$ to very high values re-

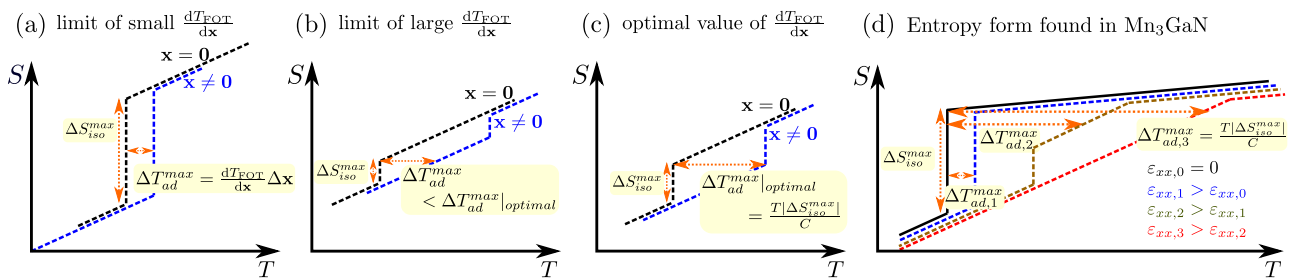


FIG. 2. Typical temperature-dependent entropy functions of magnetic materials showing a single first-order magnetic phase transition in the limit of (a) small and (b) large values of $\frac{dT_{\text{FOT}}}{dx}$. Panel (c) shows the function for the optimal value of $\frac{dT_{\text{FOT}}}{dx}$ maximizing the available adiabatic temperature change, $\Delta T_{ad}^{max}|_{\text{optimal}}$. (d) Schematics of the entropy form found in Mn_3GaN , which shows both first-order and second-order transitions, for increasing values of applied tensile strain.

duces both ΔT_{ad} and ΔS_{iso} (panel (b)), which is in fact the situation observed for Dy at T_t as shown in Fig. 1(e). Note that ΔS_{iso} is fairly small despite the first-order transition.

The optimal dependence giving the largest possible value of ΔT_{ad} is obtained at an intermediate magnitude of $\frac{dT_{\text{FOT}}}{dx}$, shown in Fig. 2(c), which provides $\Delta T_{ad}^{max}|_{\text{optimal}} = \frac{T\Delta S_{iso}^{max}}{C}$ for a substantial value of ΔS_{iso}^{max} at the transition. However, here ΔS_{iso}^{max} is far of being the largest possible isothermal entropy change available in the material. If a larger value of the isothermal entropy change is desired it directly follows from Eq. (3) that ΔT_{ad} is reduced. In section V we discuss how a qualitatively different behavior of the entropy as a function of temperature, found in the magnetically frustrated Mn_3GaN antiperovskite material¹⁰, can be used to achieve the maximum possible adiabatic temperature change $\Delta T_{ad}^{max}|_{\text{optimal}}$ ^{2,49,50}, while ΔS_{iso}^{max} itself is not constrained by the magnitude of $\Delta T_{ad}^{max}|_{\text{optimal}}$. Large values for both caloric quantities can then ensue. This desirable outcome arises from a combination of first- and second-order magnetic phase transitions produced by the application of strain and its effect on the geometrically frustrated magnetic interactions between Mn atoms. We expand on such a temperature-dependence of the entropy and compare it with the well studied limits and optimal forms of $S(T)$, shown in Fig. 2, and how the presence of a tricritical point enables hysteresis effects to be removed from half of an elastocaloric cooling cycle.

V. FRUSTRATED MAGNETISM AND OPTIMAL FORMS OF THE ENTROPY

The magnetism of systems presenting strong spin-lattice coupling can be manipulated by the application and removal of mechanical stress. Materials in which magnetic frustration plays an important role show particularly dramatic responses when they are strained. Changing their crystal symmetry and relative interatomic distances via stress application can have a substantial impact on the geometrically frustrated magnetic

interactions, which in turn strongly change the stability of frustrated and non-frustrated magnetic phases. This is the situation observed in the Mn-based antiperovskite nitride systems Mn_3GaN and Mn_3NiN ^{10,51,52}. The unstrained form of these two materials show a first-order PM-to-triangular AFM phase transition at T_N ^{53,54}, shown in Fig. 3(a), which arises from the frustrated antiferromagnetic interactions between nearest neighbor Mn atoms. The figure shows the theoretically predicted temperature-biaxial strain magnetic phase diagram of Mn_3GaN , obtained using the theory presented here¹⁰, which is qualitatively similar to the experimental diagram recently found for Mn_3NiN ⁵¹. As tensile biaxial strain is increased and the c/a ratio reduces, the triangular AFM phase distorts to form a canted triangular AFM state at low temperature. Interestingly, at higher temperatures the PM state becomes unstable to the formation of a collinear AFM phase at T_{lr} , which exhibits a very prominent shift upwards as biaxial strain increases. This collinear AFM state shows itself as the most magnetically frustrated phase in the diagram since one of its Mn sites is fully frustrated and a zero net magnetizations occurs, i.e. the corresponding orientational average of the magnetic moment vanishes, $\mathbf{m}_n = \langle \hat{\mathbf{e}}_n \rangle = \mathbf{0}$. The transitions between all these magnetic phases have different first- and second-order character, as denoted in the diagram, and the associated entropy change at T_N is giant⁵⁴. This makes Mn-based antiperovskite materials very interesting for the study of caloric effects emerging from the change of magnetism driven by mechanical stimuli, i.e. a mechanocaloric effect.

In Fig. 3(b) we show the calculated temperature dependence of the entropy, schematically shown in Fig. 2(d), the isothermal entropy change and the adiabatic temperature change obtained for Mn_3GaN on releasing the external stress as $\varepsilon_{xx} \neq 0 \rightarrow \varepsilon_{xx} = 0$. At small strains the entropy's temperature-dependent behavior corresponds to the small $\frac{dT_N}{d\sigma}$ limit, where σ is the absolute value of the biaxial tensile stress applied. This situation gives substantial values of ΔS_{iso} (see Eq. (3)) but modest ΔT_{ad} changes. However, for larger strains $S(T)$ strongly changes its behavior to resemble the temperature-dependence observed in the limit of large

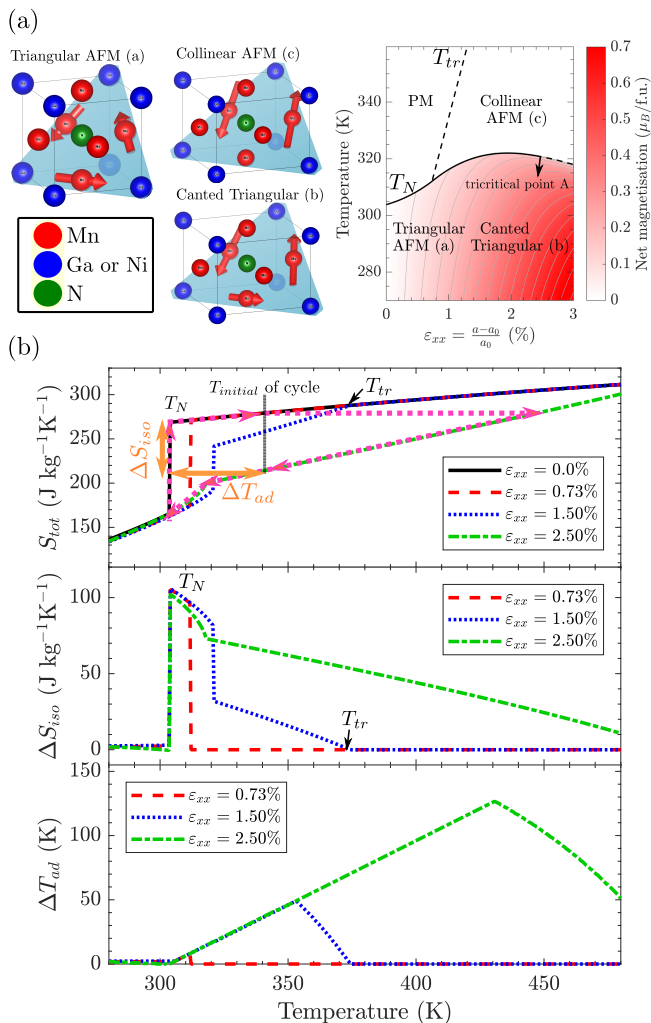


FIG. 3. (a) Temperature-strain magnetic phase diagram of Mn₃GaN, as obtained in Ref.¹⁰, for tensile values of biaxial strain ϵ_{xx} . The most stable AFM phases, triangular, canted triangular, and collinear, are also shown. Continuous(dashed) black lines mark first-(second-) order magnetic phase transitions. (b) Entropy, isothermal entropy change ΔS_{iso} , and adiabatic temperature change ΔT_{ad} in Mn₃GaN as functions of temperature and for increasing values of biaxial strain from zero to $\epsilon_{xx} = 2.5\%$, beyond the tricritical point. ΔT_{ad} is given for its magnitude obtained when strain is released, i.e. $S(T, \epsilon_{xx} \neq 0) = S(T + \Delta T_{ad}, \epsilon_{xx} = 0)$.

$\frac{dT_N}{d\sigma}$. This is a direct consequence of its approaching the tricritical point A shown in the magnetic phase diagram (Fig. 3(a)). At larger strains from this point the first-order phase transition between the collinear AFM and canted triangular AFM phases becomes second-order and co-exists together with a PM-collinear AFM second-order phase transition occurring at high temperature. The changing shape of $S(T)$ with stress application from one limiting case to the other gives rise to a somewhat triangular contour, in contrast with the rectangular one typically observed shown in Fig. 2(a-c). This automatically produces a maximum adiabatic temperature change

equal to $\Delta T_{ad}^{max} = \frac{T \Delta S_{iso}^{max}}{C}$, provided that large enough tensile strains are attained. This is the largest possible value allowed for an arbitrary magnitude of ΔS_{iso} associated with the first-order magnetic phase transition at $\epsilon_{xx} = 0$, and also equal to the optimal value for materials with a single discontinuous transition², see Fig. 2. The combination of first- and second-order magnetic phase transitions, and the presence of the tricritical point A, produces a changing entropy shape against applied field which maximizes both the isothermal entropy change and adiabatic temperature change simultaneously. A key aspect in the origin of this optimal behavior is how the instability of the PM phase to the formation of a magnetic state changes from a strong first-order with small $\frac{dT_N}{d\sigma}$ (small ϵ_{xx}) to a second-order with large $\frac{dT_N}{d\sigma}$ (large ϵ_{xx}). Here this occurs owing to the highly responsive frustrated magnetic interactions between Mn atoms to strain application¹⁰.

At $\epsilon_{xx} = 2.5\%$ a temperature span of roughly 100K above $T_N \approx 300\text{K}$ is obtained where both ΔS_{iso} and ΔT_{ad} are very large, as shown in Fig. 3(b). We highlight that the experimental magnetic phase diagram recently obtained for Mn₃NiN⁵¹ shows that 0.1% biaxial strain is enough to stabilize the collinear AFM phase at very high temperature, which is an order of magnitude smaller than our predictions. This indicates that getting close to the vicinity of the tricritical point would require the production of around 0.25% strains, which should be experimentally feasible. Finally, we point out that mechanocaloric cooling cycles using strains above the tricritical point, for example $\epsilon_{xx} = 2.5\%$ (expected to be lower in experiment), will strongly benefit from the removal of hysteresis effects on half of an elastocaloric caloric cycle. As shown for the proposed cooling cycle indicated by dotted magenta lines in the top plot of Fig. 3(b), a first-order transition is crossed only a single time every cycle owing to the second-order behavior at $\epsilon_{xx} = 2.5\%$.

VI. CONCLUSIONS

New multicaloric effects and cooling cycles in which ΔS_{iso} and ΔT_{ad} quantities are large and hysteresis losses small are highly desirable for the ongoing development of solid state cooling technologies⁵⁵. At a fundamental level the effects stem from the complexity of the interacting electronic glue in materials, how it responds and affects magnetic order, for example, and links it with other physical properties. In this article we have set out a case for *ab initio* computational materials modelling to have a key role in harnessing this physics, providing insight, sometimes being predictive and capturing trends well. We have presented theory results and compared them with experiment for caloric effects in three materials, the magnetic phase diagrams of which we had previously modelled with our DFT-DLM theory. All three materials possess both first- and second-order magnetic phase transitions as a function of T and applied stim-

ulus and we have shown how the sign and size of the caloric ΔS_{iso} and ΔT_{ad} quantities vary in the vicinity of these transitions. The link to the variation of transition temperatures with applied stimulus has also been studied. We have further exploited the rich phase diagram a Mn-rich antiperovskite nitride to propose an example of a new sort of cooling cycle in which a major source of hysteresis effects has been removed. This demonstration might motivate further exploration of the solid state cooling potential of Mn-rich materials which harbor frustrated magnetic interactions.

VII. ACKNOWLEDGEMENTS

The work was supported by EPSRC (UK) grants EP/J06750/1 and EP/M028941/1. E. M.-T. acknowledges funding from the priority programme SPP1599 "Ferroic Cooling" (Grant No. HI1300/6-2).

- ¹K. A. G. Jr, V. K. Pecharsky, and A. O. Tsokol, "Recent developments in magnetocaloric materials," *Reports on Progress in Physics* **68**, 1479 (2005).
- ²K. G. Sandeman, "Magnetocaloric materials: The search for new systems," *Scripta Materialia* **67**, 566 – 571 (2012), viewpoint Set No. 51: Magnetic Materials for Energy.
- ³X. Moya, S. Kar-Narayan, and N. D. Mathur, "Caloric materials near ferroic phase transitions." *Nat. Mater.* **13**, 439–50 (2014).
- ⁴E. Mendive-Tapia and J. B. Staunton, "Ab initio theory of the gibbs free energy and a hierarchy of local moment correlation functions in itinerant electron systems: The magnetism of the mn_3a materials class," *Phys. Rev. B* **99**, 144424 (2019).
- ⁵C. E. Patrick and J. B. Staunton, "Temperature-dependent magnetocrystalline anisotropy of rare earth/transition metal permanent magnets from first principles: The light $rcos(r = Y, La-Gd)$ intermetallics," *Phys. Rev. Materials* **3**, 101401 (2019).
- ⁶J. B. Staunton, R. Banerjee, M. d. S. Dias, A. Deak, and L. Szunyogh, "Fluctuating local moments, itinerant electrons, and the magnetocaloric effect: Compositional hypersensitivity of FeRh," *Phys. Rev. B* **89**, 054427 (2014).
- ⁷J. B. Staunton, M. dos Santos Dias, J. Peace, Z. Gercsi, and K. G. Sandeman, "Tuning the metamagnetism of an antiferromagnetic metal," *Phys. Rev. B* **87**, 060404 (2013).
- ⁸L. Petit, D. Paudyal, Y. Mudryk, K. A. Gschneidner, V. K. Pecharsky, M. Lüders, Z. Szotek, R. Banerjee, and J. B. Staunton, "Complex magnetism of lanthanide intermetallics and the role of their valence electrons: Ab initio theory and experiment," *Phys. Rev. Lett.* **115**, 207201 (2015).
- ⁹E. Mendive-Tapia and J. B. Staunton, "Theory of magnetic ordering in the heavy rare earths: Ab initio electronic origin of pair- and four-spin interactions," *Phys. Rev. Lett.* **118**, 197202 (2017).
- ¹⁰J. Zemen, E. Mendive-Tapia, Z. Gercsi, R. Banerjee, J. B. Staunton, and K. G. Sandeman, "Frustrated magnetism and caloric effects in Mn-based antiperovskite nitrides: Ab initio theory," *Phys. Rev. B* **95**, 184438 (2017).
- ¹¹B. L. Gyorffy, A. J. Pindor, J. Staunton, G. M. Stocks, and H. Winter, "A first-principles theory of ferromagnetic phase transitions in metals," *Journal of Physics F: Metal Physics* **15**, 1337 (1985).
- ¹²J. B. Staunton and B. L. Gyorffy, "Onsager cavity fields in itinerant-electron paramagnets," *Phys. Rev. Lett.* **69**, 371–374 (1992).
- ¹³C. E. Patrick and J. B. Staunton, "Rare-earth/transition-metal magnets at finite temperature: Self-interaction-corrected relativistic density functional theory in the disordered local moment picture," *Phys. Rev. B* **97**, 224415 (2018).
- ¹⁴C. E. Patrick and J. B. Staunton, "Crystal field coefficients for yttrium analogues of rare-earth/transition-metal magnets using density-functional theory in the projector-augmented wave formalism," *Journal of Physics: Condensed Matter* **31**, 305901 (2019).
- ¹⁵J. B. Staunton, A. Marmodoro, and A. Ernst, "Using density functional theory to describe slowly varying fluctuations at finite temperatures: local magnetic moments in gd and the 'not so local' moments of Ni," *Journal of Physics: Condensed Matter* **26**, 274210 (2014).
- ¹⁶Q. Chen and B. Sundman, "Calculation of debye temperature for crystalline structures—a case study on ti, zr, and hf," *Acta Materialia* **49**, 947 – 961 (2001).
- ¹⁷S. Nikitin, G. Myalikgulyev, M. Annaorazov, A. Tyurin, R. Mynydyev, and S. Akopyan, "Giant elastocaloric effect in FeRh alloy," *Physics Letters A* **171**, 234 – 236 (1992).
- ¹⁸M. P. Annaorazov, S. A. Nikitin, A. L. Tyurin, K. A. Asatryan, and A. K. Dovletov, "Anomalously high entropy change in ferh alloy," *Journal of Applied Physics* **79**, 1689–1695 (1996), <https://doi.org/10.1063/1.360955>.
- ¹⁹M. Fallot, "Les alliages du fer avec les métaux de la famille du platine," *Ann. Phys.* **11**, 291–332 (1938), <https://doi.org/10.1051/anphys/193811100291>.
- ²⁰J. van Driel, R. Coehoorn, G. J. Strijkers, E. Brück, and F. R. de Boer, "Compositional dependence of the giant magnetoresistance in $fe_{xrh}1-x$ thin films," *Journal of Applied Physics* **85**, 1026–1036 (1999), <https://doi.org/10.1063/1.369224>.
- ²¹Y. Kobayashi, K. Muta, and K. Asai, "The hall effect and thermoelectric power correlated with the giant magnetoresistance in modified FeRh compounds," *Journal of Physics: Condensed Matter* **13**, 3335–3346 (2001).
- ²²S. Maat, J.-U. Thiele, and E. E. Fullerton, "Temperature and field hysteresis of the antiferromagnetic-to-ferromagnetic phase transition in epitaxial ferh films," *Phys. Rev. B* **72**, 214432 (2005).
- ²³C. Stamm, J.-U. Thiele, T. Kachel, I. Radu, P. Ramm, M. Kosuth, J. Minár, H. Ebert, H. A. Dürr, W. Eberhardt, and C. H. Back, "Antiferromagnetic-ferromagnetic phase transition in ferh probed by x-ray magnetic circular dichroism," *Phys. Rev. B* **77**, 184401 (2008).
- ²⁴I. Suzuki, T. Naito, M. Itoh, T. Sato, and T. Taniyama, "Clear correspondence between magnetoresistance and magnetization of epitaxially grown ordered ferh thin films," *Journal of Applied Physics* **109**, 07C717 (2011), <https://doi.org/10.1063/1.3556754>.
- ²⁵M. A. de Vries, M. Loving, A. P. Mihai, L. H. Lewis, D. Heiman, and C. H. Marrows, "Hall-effect characterization of the metamagnetic transition in FeRh," *New Journal of Physics* **15**, 013008 (2013).
- ²⁶V. L. Moruzzi and P. M. Marcus, "Antiferromagnetic-ferromagnetic transition in ferh," *Phys. Rev. B* **46**, 2864–2873 (1992).
- ²⁷M. E. Gruner, E. Hoffmann, and P. Entel, "Instability of the rhodium magnetic moment as the origin of the metamagnetic phase transition in $\alpha - FeRh$," *Phys. Rev. B* **67**, 064415 (2003).
- ²⁸L. M. Sandratskii and P. Mavropoulos, "Magnetic excitations and femtomagnetism of ferh: A first-principles study," *Phys. Rev. B* **83**, 174408 (2011).
- ²⁹O. N. Mryasov, "Magnetic interactions and phase transformations in $fem\ m = (pt, rh)$ ordered alloys," *Phase Transitions* **78**, 197–208 (2005), <https://doi.org/10.1080/01411590412331316591>.
- ³⁰P. M. Derlet, "Landau-heisenberg hamiltonian model for ferh," *Phys. Rev. B* **85**, 174431 (2012).
- ³¹D. W. Cooke, F. Hellman, C. Baldasseroni, C. Bordel, S. Moyerman, and E. E. Fullerton, "Thermodynamic measurements of fe-rh alloys," *Phys. Rev. Lett.* **109**, 255901 (2012).
- ³²E. Stern-Taulats, A. Planes, P. Lloveras, M. Barrio, J.-L. Tamarit, S. Pramanick, S. Majumdar, C. Frontera, and L. Mañosa, "Barocaloric and magnetocaloric effects in $Fe_{49}Rh_{51}$," *Phys. Rev. B* **89**, 214105 (2014).

- ³³A. Gràcia-Condal, E. Stern-Taulats, A. Planes, and L. Mañosa, “Caloric response of $\text{Fe}_{49}\text{Rh}_{51}$ subjected to uniaxial load and magnetic field,” *Phys. Rev. Materials* **2**, 084413 (2018).
- ³⁴J. Jensen and A. R. Mackintosh, *Rare Earth Magnetism, Estructure and Excitations* (Clarendon, Oxford, 1991).
- ³⁵V. I. Zverev, A. M. Tishin, A. S. Chernyshov, Y. Mudryk, K. A. G. Jr, and V. K. Pecharsky, “Magnetic and magnetothermal properties and the magnetic phase diagram of high purity single crystalline terbium along the easy magnetization direction,” *Journal of Physics: Condensed Matter* **26**, 066001 (2014).
- ³⁶D. C. Jiles, S. B. Palmer, D. W. Jones, S. P. Farrant, and K. A. G. Jr, “Magnetoelastic properties of high-purity single-crystal terbium,” *Journal of Physics F: Metal Physics* **14**, 3061 (1984).
- ³⁷A. V. Andrianov, O. A. Savel’eva, E. Bauer, and J. B. Staunton, “Squeezing the crystalline lattice of the heavy rare-earth metals to change their magnetic order: Experiment and ab initio theory,” *Phys. Rev. B* **84**, 132401 (2011).
- ³⁸G. I. Kataev, M. R. Sattarov, and A. M. Tishin, “Influence of commensurability effects on the magnetic phase diagram of terbium single crystals,” *physica status solidi (a)* **114**, K79–K82 (1989).
- ³⁹R. Herz and H. Kronmüller, “Field-induced magnetic phase transitions in dysprosium,” *Journal of Magnetism and Magnetic Materials* **9**, 273 – 275 (1978).
- ⁴⁰A. S. Chernyshov, A. O. Tsokol, A. M. Tishin, K. A. Gschneidner, and V. K. Pecharsky, “Magnetic and magnetocaloric properties and the magnetic phase diagram of single-crystal dysprosium,” *Phys. Rev. B* **71**, 184410 (2005).
- ⁴¹J. Yu, P. R. LeClair, G. J. Mankey, J. L. Robertson, M. L. Crow, and W. Tian, “Exploring the magnetic phase diagram of dysprosium with neutron diffraction,” *Phys. Rev. B* **91**, 014404 (2015).
- ⁴²V. I. Zverev, A. M. Tishin, Z. Min, Y. Mudryk, K. A. G. Jr, and V. K. Pecharsky, “Magnetic and magnetothermal properties, and the magnetic phase diagram of single-crystal holmium along the easy magnetization direction,” *Journal of Physics: Condensed Matter* **27**, 146002 (2015).
- ⁴³J. R. Gebhardt and N. Ali, “Magnetic phase diagrams of holmium determined from magnetoresistance measurements,” *Journal of Applied Physics* **83**, 6299–6301 (1998), <https://doi.org/10.1063/1.367685>.
- ⁴⁴M. Rosen, “Elastic moduli and ultrasonic attenuation of gadolinium, terbium, dysprosium, holmium, and erbium from 4.2 to 300K,” *Phys. Rev.* **174**, 504–514 (1968).
- ⁴⁵S. B. Palmer, “Debye temperatures of holmium and dysprosium from single crystal elastic constant measurements,” *Journal of Physics and Chemistry of Solids* **31**, 143 – 147 (1970).
- ⁴⁶V. Y. Bodryakov, A. A. Povzner, and O. G. Zelyukova, “Magnetic contribution to the Debye temperature and the lattice heat capacity of ferromagnetic rare-earth metals (using gadolinium as an example),” *Physics of the Solid State* **41**, 1138–1143 (1999).
- ⁴⁷A. M. Tishin and Y. I. Spichkin, *The Magnetocaloric Effect and its Applications*, Vol. 6 (2003).
- ⁴⁸E. Bonnot, R. Romero, L. Mañosa, E. Vives, and A. Planes, “Elastocaloric effect associated with the martensitic transition in shape-memory alloys,” *Phys. Rev. Lett.* **100**, 125901 (2008).
- ⁴⁹M. D. Kuz’min, K. P. Skokov, D. Y. Karpenkov, J. D. Moore, M. Richter, and O. Gutfleisch, “Magnetic field dependence of the maximum adiabatic temperature change,” *Applied Physics Letters* **99**, 012501 (2011), <https://doi.org/10.1063/1.3607279>.
- ⁵⁰V. I. Zverev, A. M. Tishin, and M. D. Kuz’min, “The maximum possible magnetocaloric ΔT effect,” *Journal of Applied Physics* **107**, 043907 (2010), <https://doi.org/10.1063/1.3309769>.
- ⁵¹D. Boldrin, F. Johnson, R. Thompson, A. P. Mihai, B. Zou, J. Zemen, J. Griffiths, P. Gubeljak, K. L. Ormandy, P. Manuel, D. D. Khalyavin, B. Ouladdiaf, N. Qureshi, P. Petrov, W. Branford, and L. F. Cohen, “The biaxial strain dependence of magnetic order in spin frustrated mn_3nin thin films,” *Advanced Functional Materials* **29**, 1902502 (2019), <https://onlinelibrary.wiley.com/doi/pdf/10.1002/adfm.201902502>.
- ⁵²D. Boldrin, E. Mendive-Tapia, J. Zemen, J. B. Staunton, T. Hansen, A. Aznar, J.-L. Tamarit, M. Barrio, P. Lloveras, J. Kim, X. Moya, and L. F. Cohen, “Multisite exchange-enhanced barocaloric response in mn_3NiN ,” *Phys. Rev. X* **8**, 041035 (2018).
- ⁵³P. L’Héritier, D. Fruchart, R. Madar, and R. Fruchart, *Alloys and Compounds of d-Elements with Main Group Elements. Part 2*, Landolt-Börnstein - Group III Condensed Matter, edited by H. P. J. Wijn, New Series III/19c (Springer-Verlag, Berlin, Heidelberg, 1988).
- ⁵⁴D. Matsunami, A. Fujita, K. Takenaka, and M. Kano, “Giant barocaloric effect enhanced by the frustration of the antiferromagnetic phase in Mn_3GaN ,” *Nature Materials* **14**, 73 (2015).
- ⁵⁵F. Scheibel, T. Gottschall, A. Taubel, M. Fries, K. P. Skokov, A. Terwey, W. Keune, K. Ollefs, H. Wende, M. Farle, M. Acet, O. Gutfleisch, and M. E. Gruner, “Hysteresis design of magnetocaloric materials—from basic mechanisms to applications,” *Energy Technology* **6**, 1397–1428 (2018), <https://onlinelibrary.wiley.com/doi/pdf/10.1002/ente.201800264>.